PAPER

The visibility of IQHE at sharp edges: experimental proposals based on interactions and edge electrostatics

New Journal of Physics
The open-access journal for physics

The visibility of IQHE at sharp edges: experimental proposals based on interactions and edge electrostatics

U Erkarslan[1], G Oylumluoglu[1], M Grayson[2] and A Siddiki[3,4]

[1] Department of Physics, Faculty of Arts and Sciences, Mugla University, 48170-Kotekli, Mugla, Turkey

[2] Electrical Engineering and Computer Science, Northwestern University, Evanston, IL 60208, USA

[3] Department of Physics, Faculty of Sciences, Istanbul University, 34134 Vezneciler, Istanbul, Turkey

E-mail: afifsiddiki@gmail.com

New Journal of Physics **14** (2012) 023015 (26pp)
Received 24 August 2011
Published 6 February 2012
Online at http://www.njp.org/
doi:10.1088/1367-2630/14/2/023015

Abstract. The influence of the incompressible strips on the integer quantized Hall effect (IQHE) is investigated, considering a cleaved-edge overgrown (CEO) sample as an experimentally realizable sharp edge system. We propose a set of experiments to clarify the distinction between the large-sample limit when bulk disorder defines the IQHE plateau width and the small-sample limit smaller than the disorder correlation length, when self-consistent edge electrostatics define the IQHE plateau width. The large-sample or bulk quantized Hall (QH) regime is described by the usual localization picture, whereas the small-sample or edge regime is discussed within the compressible/incompressible strips picture, known as the screening theory of QH edges. Utilizing the unusually sharp edge profiles of the CEO samples, a Hall bar design is proposed to manipulate the edge potential profile from smooth to extremely sharp. By making use of a side-gate perpendicular to the two-dimensional electron system, it is shown that the plateau widths can be changed or even eliminated altogether. Hence, the visibility of IQHE is strongly influenced when adjusting the edge potential profile and/or changing the dc current direction under high currents in the nonlinear transport regime. As a second investigation, we consider two different types of ohmic

[4] Author to whom any correspondence should be addressed.

contacts, namely highly transmitting (ideal) and highly reflecting (non-ideal) contacts. We show that if the injection contacts are non-ideal, but still ohmic, it is possible to measure directly the non-quantized transport taking place at the bulk of the CEO samples. The results of the experiments we propose will clarify the influence of the edge potential profile and the quality of the contacts, under QH conditions.

Contents

The integer quantized Hall effect (IQHE) is observed in a two-dimensional electron gas (2DEG) subjected to a strong perpendicular magnetic field B, with signatures in the longitudinal R_L and transverse R_H resistances [1]. At certain magnetic field intervals, R_L vanishes and R_H is quantized. Surprisingly, the theories that elucidate the IQHE are still under discussion, even today [2]. Two main schools have emerged in explaining the IQHE, namely the bulk [3, 4] and the edge [5–7] pictures. They are believed to contrast with each other in describing the current distribution. The former assumes that the transport is at the bulk and quantization is determined by localization effects, whereas the latter neglects the effects of disorder and assumes 1D ballistic channels at the edge, carrying the quantized current. Although early arguments took a contrasting view [7], it is currently widely accepted that edge currents flow losslessly within the incompressible strips [8, 9].

The compressible/incompressible strips result electrostatically from a quantizing magnetic field in combination with self-consistent direct Coulomb interactions under the constraint of electrostatic boundary conditions. The magnetic field quantizes the density of states (DOS) into highly degenerate Landau levels separated from each other by cyclotron or Zeeman energy gaps. If the Fermi energy is pinned to one of these Landau levels for a finite width parallel to the edge of the sample, the strip is called compressible, due to the high degeneracy at the DOS. If the Fermi energy resides *between* Landau levels, the strip is called incompressible, since there are no available states at the Fermi energy for the entire width of this strip. It is

standard to define a dimensionless parameter called the filling factor ν, which gives the ratio of the electron density $n_{\rm el}$ to the density of magnetic flux quanta n_Φ. One can express the filling factor as $\nu = n_{\rm el}/n_\Phi = 2\pi\ell_B^2 n_{\rm el}$, where $\ell_B = \sqrt{\hbar/eB}$ is the magnetic length. The local version of the filling factor is defined by $\nu(x, y) = 2\pi\ell^2 n_{\rm el}(x, y)$, where $n_{\rm el}(x, y)$ is the electron number density, locally. An integer ν (and also $\nu(x, y)$ locally) implies that all the Landau levels below the Fermi energy are fully occupied; hence, the system is in an incompressible state. Otherwise the Landau level is pinned to the Fermi energy and is partially occupied; therefore the system is compressible. The properties of these strips have been investigated intensively in the literature, both theoretically [7, 10–16] and experimentally [17–25]. The theoretical investigations, known as the screening theory, aim to clarify the effects of the boundary electrostatics [7, 10–12], temperature [13, 14] and current [15, 16] on the formation of incompressible strips. More recently, the behavior of the incompressible strips near the contacts was investigated experimentally [22] and theoretically [26]. These investigations helped to resolve the long-standing question of what characteristics define an ideal contact. However, the effect of electrostatic boundary conditions on the formation of incompressible strips far from contacts remains unresolved.

The objective of this work is twofold. Firstly, we explore the existence of incompressible strips in the presence of infinitely sharp confinement walls. Our discussion is based on the existing experimental literature [19, 20, 22, 25] and semi-classical calculations [9, 16]. We show that these strips vanish at sharp edges due to overlap of the quantum mechanical wavefunctions across the incompressible strip remnant. Exploiting the findings of the interaction theory of the IQHE [9] and local probe experiments [19], we claim that the longitudinal resistance evolves differently on sharp and smooth edges when transitioning between quantized Hall effect (QHE) plateaux. Secondly, we show that the Hall resistance is non-quantized even at the plateau regime due to the evanescent bulk current. This behavior depends on the contact quality. This paper is organized as follows. In the following section, we briefly introduce the material and geometrical properties of the sample proposed here. The first part of section 2 is spared for the formulation of the screening theory, where we also present the results of self-consistent numerical calculations. The second part highlights the essentials of local probe and CEO experiments, followed by a brief discussion of the transport model (section 2.3). The effect of ideal/non-ideal contacts on transport, considering a varying magnetic field, is investigated in section 3. There we show that, in the case of ideal contacts, one expects to observe differences between generic and CEO samples when measuring either the local electrochemical or the longitudinal resistances. For the non-ideal contacts we predict that some of the current is scattered to bulk due to the absence of an incompressible strip at the CEO. Hence, the Hall resistance is not quantized even at the plateau regime. We discuss the effects of the sweeping direction and the orientation of magnetic field on transport, which induces a hysteresis in section 4.

1. The wafer and the sample geometry

In standard molecular beam epitaxy (MBE), the crystal is grown in the z-direction layer by layer. However, well-established experimental techniques are able to grow materials in different crystal directions in sequential steps. As a first step a usual MBE growth process is performed; then the crystal is removed from the chamber, thinned, scribed, returned to the chamber mounted at a 90° angle and then cleaved *in situ* and regrown. This process is known as the cleaved edge overgrowth (CEO) technique [27]. The CEO samples are used to investigate the edge properties

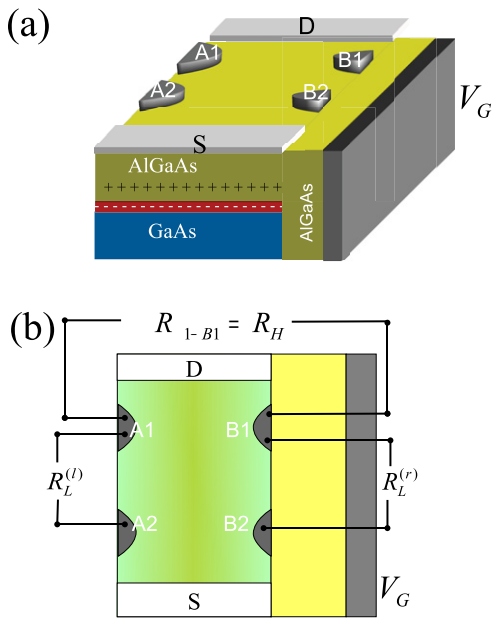

Figure 1. The side-view (a) and top-view (b) projections of the sample design. The Hall bar is defined by etching on the left-hand side (lhs), generating a relatively smooth potential profile, whereas on the right-hand side (rhs) the CEO edge serves as a steep potential. The steepness is manipulated by the side gate (gray region), by applying a negative potential. The illustration is not to scale.

of the quantum Hall systems via momentum-resolved tunneling experiments, utilizing the second 2DEG residing perpendicular to the Hall system [20, 21]. These tunneling experiments show that the CEO edge provides an extreme sharp potential approximating an infinite wall. The sample structure proposed here does not involve tunneling, but rather probes the sharpness of the QHE edges via transport alone.

A schematic representation of the crystal is depicted in figure 1. The Hall bar lies in the xy-plane, obtained by usual MBE growth, whereas on the rhs of the crystal an additional AlGaAs layer is grown. This is the CEO edge and is capped by a metallic gate. The gate covers all the surface and is kept at a fixed potential V_G. To measure the global resistances and to drive an external current I through the 2DEG, ohmic contacts are deposited on the top surface of the system. The voltage probe contacts are labeled A1, A2, B1 and B2 to measure R_H and R_L, whereas the current contacts S and D denote the source and the drain. In our discussion of the visibility of the IQHE, we will describe transport in such a CEO sample. We consider a system where at one edge (CEO edge) a side gate resides; meanwhile, the opposing edge is defined by the standard etching process.

2. The formulation of the screening theory, relevant experiments and the complementary transport model

This section aims to provide the necessary theoretical and experimental background to discuss the transport properties of the proposed CEO samples. Our theory discussion consists of two parts: first, we reintroduce the analytical formulation behind the self-consistent screening

calculations and discuss the existence of incompressible strips. The second part presents the numerical results. Next, we summarize the observations of two sets of experiments relevant for our discussion. The distinction between the small-sample edge IQHE and the large-sample bulk IQHE is clarified after we discuss the results of local probe experiments and corresponding theory results. In the last part, we briefly recall the complementary transport calculations utilized by the screening theory to elucidate IQHE.

2.1. The calculation scheme

Here, we briefly reintroduce the calculation scheme for obtaining electrostatic potential and electron density distributions of a 2DEG. Let us assume that the electrons are confined at the xy-plane due to an external potential $V_{\mathrm{conf}}(x, y)$, which results from remote donors and metallic gates. At zero temperature and in the absence of a perpendicular magnetic field, this confinement potential will be filled with electrons up to the Fermi energy E_{F} continuously by virtue of constant DOS D_0 $(= m/\pi\hbar^2)$, specific to 2D. Taking into account the mutual (direct) Coulomb interaction within a mean-field approximation, one obtains the Hartree potential (energy) as

$$V_{\mathrm{Ha}}(x, y) = \frac{e^2}{\kappa} \int_A n_{\mathrm{el}}(x, y) K(x, y; x', y') \mathrm{d}x\, \mathrm{d}y, \tag{1}$$

where κ is the dielectric constant of the material, A is the area where the 2DEG is confined and $K(x, y; x', y')$ is the solution of the Poisson equation to be specified for the given boundary conditions. The closed form of the kernel resembling the smooth boundary conditions was discussed by Chklovskii *et al* [7] considering in-plane gates and translational invariance. In addition, the form of the kernel in the presence of gates perpendicular to the 2DEG similar to a both sides CEO system is also discussed in the literature [28]. The closed form of the kernel in the case of perpendicular gates is given by

$$K_{\perp}(x, x') = -\ln\left(\frac{\cos^2\frac{\pi}{4d}(x + x') + \gamma^2}{\sin^2\frac{\pi}{4d}(x - x') - \gamma^2}\right), \tag{2}$$

where d is the sample width and $\gamma = \sinh(\pi z/4d)$ gives the z-dependence. However, a closed form for the mixed boundary conditions, i.e. a realistic CEO sample, does not exist and requires numerical calculations, as provided in the following discussion. Note that similar expressions are available in the textbook of Morse and Feshbach considering two dimensions, but, unfortunately, they are limited to periodic boundary conditions [29]. As a direct consequence, the total electrostatic potential energy that an electron experiences is

$$V_{\mathrm{T}}(x, y) = V_{\mathrm{conf}}(x, y) + V_{\mathrm{Ha}}(x, y). \tag{3}$$

In the next step, one should calculate the new electron distribution regarding this potential by solving the single-particle Schrödinger equation. For the moment, let us assume a generic Hamiltonian H and depict the energy eigen functions by $\phi_\alpha(x, y)$ and eigen values by E_α. The effect of temperature on electron occupation can be incorporated utilizing the Fermi–Dirac function $f(E_\alpha, E_{\mathrm{F}}, T)$; then the electron density distribution is described as

$$n_{\mathrm{el}}(x, y) = \sum_\alpha |\phi_\alpha(x, y)|^2 f(E_\alpha, E_{\mathrm{F}}, T). \tag{4}$$

Let us specify H to be the single-particle Hamiltonian of a spinless electron subjected to a perpendicular magnetic field, given by

$$H = H_B = \frac{1}{2m}\left(\mathbf{p} - \frac{e}{c}\mathbf{A}(x, y)\right)^2 + V_{\mathrm{T}}(x, y), \tag{5}$$

where $\mathbf{p}$ is the momentum and $\mathbf{A}(x, y)$ is the vector potential generating the magnetic field. Here, we assume a translational invariance and the vector potential is expressed in the Landau gauge. If we neglect the potential term for the moment, then the solution of the Schrödinger equation gives the energy eigen values to be $E_{n,X} = \hbar\omega_{\mathrm{c}}(n + 1/2)$, known as the Landau levels, and the wavefunctions as $\phi_{n,X}(x, y) = N \exp(\mathrm{i}ky) \exp(-(x - X)^2/2\ell_B^2) H_n((x - X)/\ell_B)$. Here, n is the Landau level index, N is a normalization factor, k is the quasi-continuous momentum in y, X $(= -\ell_B^2 k)$ specifies the orbit-center coordinate and $\omega_{\mathrm{c}} = eB/m$ is the cyclotron frequency. Since the eigen energies and values are known, one can obtain the electron density by equation (4). Note that, for smoothly varying potential, these eigen values and functions remain unchanged with correction to the energy eigen values. This approach is known as the Thomas–Fermi approximation.

Now one can calculate the new potential depending on the new electron distribution via solving the Poisson equation. This procedure requires numerical self-consistency and is a formidable task in general. Despite this difficulty, such a numerical algorithm is available, which we also discuss in the following. However, we first reintroduce the non-self-consistent analytical scheme to base our discussion on a simpler ground.

2.1.1. The non-self-consistent analytical approach. To surpass the complications due to numerical self-consistency, Chklovskii *et al* [7] proposed an analytical calculation scheme to obtain potential and electron density distributions based on electrostatic arguments. There, the solution of the Poisson equation is obtained by the use of holomorphic functions considering in-plane metallic gates at the sides. For this boundary condition the form of the kernel $K(x, y; x', y')$ is well discussed in the literature and is given by

$$K(x, x') = \ln\left|\frac{\sqrt{(d^2 - x^2)(d^2 + x^2)} + d^2 - xx'}{(x - x')d}\right|, \tag{6}$$

where a translational invariance is assumed in the y-direction. The details of the calculation can be found in [7]. The commonly used Thomas–Fermi approximation is invoked, which is adequate if the external potential varies smoothly within the magnetic length. In addition, the wavefunctions are replaced by Dirac delta functions. It is assumed *a priori* that screening is perfect at the compressible strips and poor at the incompressible strips. Hence, the external potential is completely screened at the compressible strips and the total potential profile there is flat. At the compressible strips the density profile resembles that without B field, given by

$$n_{\mathrm{el}}(x) = n_0\left(\frac{x - l_{\mathrm{d}}}{x + l_{\mathrm{d}}}\right)^{1/2}, \tag{7}$$

via the solution of the Poisson equation. Here, n_0 is the bulk electron density and l_{d} is the depletion length determined by the potential at the in-plane gate [7]. In contrast, at the dipolar incompressible strips the potential varies by an amount of cyclotron energy $\hbar\omega_{\mathrm{c}}$, whereas the density remains constant. Under these assumptions the width of the dipole incompressible strip

is given by [7]

$$a_n = \sqrt{\frac{2\kappa\,\Delta E}{\pi^2 e^2\,\mathrm{d}n(x)/\mathrm{d}x|_{x=x_n}}}, \tag{8}$$

where ΔE is the single-particle energy gap ($=\hbar\omega_c$, assuming spin degeneracy). In generic samples, the electron density distribution varies smoothly starting from the depleted region at the edge. Hence, the derivative of the electron density with respect to the spatial coordinate is small, which in turn determines the width of the incompressible strip. For sufficiently weak confining electric fields, these dipole strips are so wide that they effectively isolate the compressible strips on either side, and these dipole strips earn the name incompressible strips, as they represent a strip where no screening can take place.

As mentioned, the Thomas–Fermi approximation is viable only if the potential varies slowly on the scale of magnetic length; therefore the TFA becomes questionable if the strip width becomes comparable to ℓ_B. The full self-consistent quantum mechanical treatment of the electron density within a mean field approximation shows that the dipole strips cease to be incompressible for all magnetic field strengths [9, 30]. In fact, the collapse of the incompressible strips can be readily seen considering the effect of (local) external electric fields within the strip [31]. It is straightforward to show that the external electric field within the strip broadens the Dirac delta-shaped Landau DOS and the resulting local DOS assumes the form

$$D(E, X(E)) = \frac{1}{2\pi\ell_B^2}\sum_n \frac{1}{eE_x\ell_B}|\phi_n(X(E))|^2, \tag{9}$$

where $E_x = \frac{1}{e}\frac{\hbar\omega_c}{a_n}$ is the field at the strip and $X(E)$ is the normalized coordinate, which depends on energy. Hence, if the electric field at the strip becomes large (i.e. if the strip becomes narrow $a_n \sim \ell_B$, since the potential variation is fixed at $\hbar\omega_c$), then the adjacent Landau levels overlap, at the energy scales $eE_x\ell_B \sim \hbar\omega_c$. If this condition is satisfied the strip collapses, and disorder can easily scatter charge from the compressible region on one side to that on the other. In other words, the dipole strip has become too narrow and is able to screen electric fields within its width.

Such a result contrasts with 1D edge channel theories [6], which predict that more than one channel should always exist for $\nu > 4$. The collapse of (narrow) incompressible strips described here is due to the finite extent of the wavefunctions. The wavefunctions can tunnel across the strip when the width of the incompressible strip becomes comparable with the quantum mechanical length scales. These scales are set by the B field such as the magnetic length (width of the wavefunction) and by the Fermi wavelength, defining the thermodynamic length scale. Note that the mentioned length scales are of the same order in typical measurements with electron densities similar to $n_{\mathrm{el}} \approx 3.0 \times 10^{11}\,\mathrm{cm}^{-2}$ (corresponding to $\lambda_F \approx 25$–$35\,\mathrm{nm}$) and at intermediate B fields ($B \approx 5\mathrm{T}$, $\ell_B \approx 20\,\mathrm{nm}$).

The above vanishing of the incompressible strips applies also to the CEO sample; however, one should take care of boundary conditions imposed by the sharp edge. Here, one can use the semi-classical quantization of the skipping orbits for an initial estimation of the collapse of incompressible strips [32, 33]. It is possible to show analytically that the gapped regions between the levels are confined to an interval in the physical space, which is smaller than the magnetic length. Hence, electrostatically it is not possible to have incompressible strips at sharp edges. In addition to these arguments, the numerical investigations show that there are no incompressible strips at all if an infinite wall is considered at the edges of the sample [34].

We will show this situation in the following, where we also perform quantum mechanical calculations using computational techniques.

It is important to mention that the spin generalized calculation schemes are available in the literature. In the early analytical calculations of Dempsey *et al* [35], the effect of electron–electron interactions on spin polarization was investigated, whereas Zozoulenko and co-workers utilized the density functional approach to tackle a similar problem [36]. One can extend our above scheme to study the spin-dependent behavior using these approaches. However, the important concepts of this paper do not require consideration of the spin degree of freedom, so the simpler spinless case will be addressed here.

2.1.2. The self-consistent numerical calculations. This section is devoted to investigating the effects of boundary conditions on the electronic distribution, considering the CEO sample. We solve the 3D Poisson equation self-consistently, in the classical domain, where finite widths of the wavefunctions are not taken into account. The boundary conditions are defined purely by electrostatics and the 2DEGs are included to the calculations as 2D charged planes. Here, we first assume vanishing temperature and zero B field to obtain initial conditions. The inset of figure 2(a) shows a typical sample profile. We consider a crystal that is grown first in the z direction (i.e. [100]), then cleaved at $x = 340$ nm and the new material is grown in the x-direction, [010]. Note that the side gate resides at $x = 0$. The corresponding charge distribution and electrostatic potential profiles are shown in figure 2, where different potentials are applied to the side gate. The top surface of the crystal is assumed to be pinned to the mid gap of GaAs. As depicted in the schematic drawing, the system is delta doped by two silicon layers, which provide electrons for the quantum wells. The 3D Poisson equation is solved by the fourth-order grid technique, where successive over-relaxation is used for the iteration process [12, 37]. The potential and charge distributions of the parallel electron layer present the expected sharp variation at the cleaved edge, for small positive (solid line) and negative (broken line) side-gate potentials. At a larger negative voltage, the sharp features at the CEO edge is washed out (dash-dotted line) and the smooth edge is recovered. To compare the self-consistent density profiles with Chklovskii distribution (i.e. equation (4)), we also plot the non-self-consistent density profile in figure 2(a) (thin solid line). One can clearly see that the Chklovskii model fails to describe the calculated edge profile even under depletion [11, 25].

Once the density and potential profiles are known, it is somewhat easier to calculate the profiles at finite magnetic field. Since the density distribution is modified only at the incompressible regions and remains almost unchanged at compressible regions. Indeed, one can estimate the widths and the spatial positions of the incompressible strips simply from equation (4) using the electrostatic stability argument. Nevertheless, for numerical calculations one starts with $T = 0$, $B = 0$ profiles, increases the temperature, then adds the quantizing magnetic field via DOS and decreases the temperature step by step till the numerical accuracy is obtained. Further details of the self-consistent calculation scheme can be found in the literature, which is applied successfully to systems that assume translational invariance in the y-direction, considering single layers [9, 15, 28, 38, 39], double layers [40–42] and actual 2D systems [12, 26, 43]. This approach is known as the screening theory and its predictions are confirmed experimentally [24, 25, 44–48].

The paramount outcome of the self-consistent calculations is that the 2DEG separates into compressible strips separated by dipole strips and that only in weak confining electric fields the dipole strips are wide enough to constitute incompressible strips. The existence of

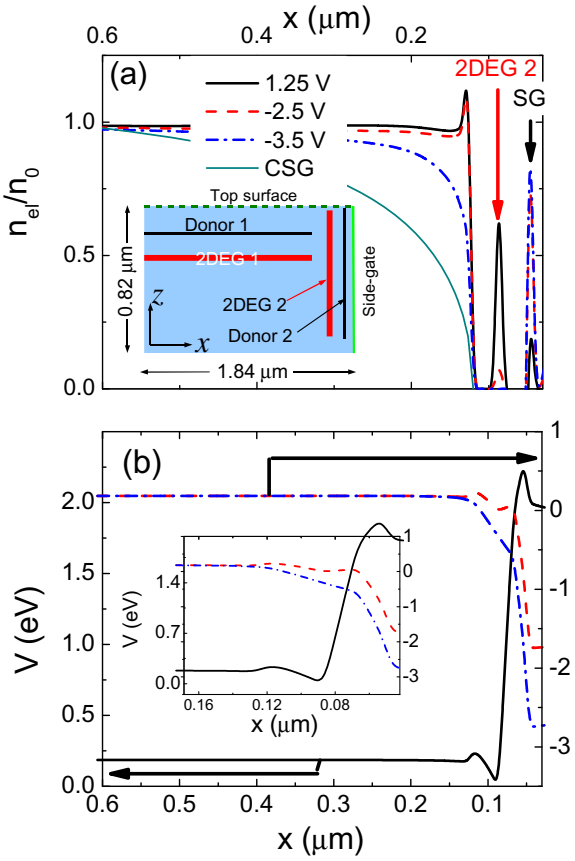

Figure 2. The results of 3D calculations depicting (a) the electron density distribution of the parallel layer (2DEG 1) and (b) the total potential profile as a function of lateral coordinate. Inset in (a) shows the schematic presentation of the CEO crystal. In the first growth donors are placed 96 nm above the 2DEG, whereas in the second growth donors are place 48 nm above the second 2DEG. Both the top and side surfaces are covered by metallic gates to manipulate the electron densities, in particular the side gate allows us to change the CEO edge from sharp to smooth. The peaks at the electron density reflect the positions of the charges at the side gate (SG) and perpendicular 2DEG (2DEG 2). The inset in (b) focuses on potential distribution at the sharp edge.

incompressible strips at low-temperature, strong-magnetic field and high-mobility samples in the small-sample limit strongly depends on the boundary conditions. Therefore, in what follows, we assume that the incompressible strip does not exist at the CEO edge, as supported by the above calculations and experiments that we discuss next. On the other hand, the properties of the incompressible strips at the 'soft' edge and bulk are determined by disorder broadened Landau levels together with temperature. In addition, our discussion on the effects of the CEO edge is qualitatively independent of the properties of the soft edge, and self-consistent calculations are not necessary since the model for each edge is known from the above arguments. Such calculations would be helpful for comparison only after a specific experimental geometry for the proposed CEO experiment has been realized.

Next, we discuss the essential findings of relevant experiments and highlight their relation to the theoretical results mentioned above.

2.2. *Relevant experiments*

The results of the above-mentioned theoretical results are confirmed by numerous experiments; however, we would like to highlight two of them in the following. An important set of experiments is the local probe measurements of the electrochemical potential distribution considering a narrow 2DEG [18, 19, 22]. Here, a scanning force microscope is utilized to investigate the local potential distribution within the 2DEG. A schematic representation resembling the experimental findings is shown in figure 3(a). It is reported that at the plateau-to-plateau transitions the position-dependent electrochemical potential $\mu(x, y)$ varies linearly (recovering the classical Hall effect) across the sample, named as type I.[5] In this regime, the current flows from the entire (compressible) system as if in a metal. No incompressible regions or strips are observed. Once the bulk filling factor is in close proximity to an integer, it is observed that $\mu(x, y)$ varies in a highly nonlinear manner, mimicking an inclined S. Here, the system is in the IQHE regime ($2.0 \lesssim \nu \lesssim 2.1$). The corresponding electrochemical potential distribution, simulating the experimental observations, is shown in figure 3(a)—type II. This behavior suggests that the current is flowing in a single bulk incompressible region [15, 19]. We name this regime the bulk IQHE, and note that the bulk can be disorderless as shown in the figure or it can have disorder fluctuations smaller than the gap energy. This description is consistent with the disorder picture of the IQHE [4], but it is important to note that disorder is not a prerequisite for observing a plateau in the quantum Hall effect. As a third type, a strong potential variation is observed at the edges, where two incompressible strips reside. Meanwhile, the potential is flat at the bulk. The observations suggest that the excess current is flowing from these strips. The strips are found to be parallel to the edges, far from the contacts. We call this regime the edge IQHE regime, where the properties of the strips are determined mainly by the electrostatics of the edges. Interestingly, one observes either a transition regime from type III to type I or a transition from type III to type IV and then again to type I. In the first case, the potential varies approximately in a linear manner both at the bulk and at the edges with different slopes (type IV); meanwhile, global resistances show that the system is just outside of the IQHE regime. In the latter case, the potential variations at the edges of type IV regime correspond to an incompressible strip, where it is called an evanescent incompressible strip [24]. At this interval, the strip is wider than the magnetic length ($\ell_B \lesssim 20$ nm), but, narrower than the Fermi wavelength ($\lambda_F \sim 25$–35 nm). The corresponding incompressible strip and current distributions are shown in figures 3(b)–(e). The results of rigorous self-consistent calculations have been published elsewhere [26, 49]; however, below we will provide a brief discussion that describes how to obtain current distribution from local filling factors.

Regarding the infinite walls as the boundary, the most relevant experiments are the ones that utilize CEO edges [20, 21]. At the CEO crystals, it is shown that no incompressible strips reside at the CEO edge, by momentum-resolved tunneling measurements. Using the perpendicular quantum well, one can tunnel into the edge of the quantum Hall bar and probe the momentum matching conditions depending on the magnetic field and the energy of the probing electrons belonging to the quantum well. It is explicitly shown that the Chklovskii incompressible strip picture [7] breaks down at extremely sharp boundary conditions [21].

[5] For a consistency check see figure 1 of [15], for the magnetic field interval $\nu < 1.96$.

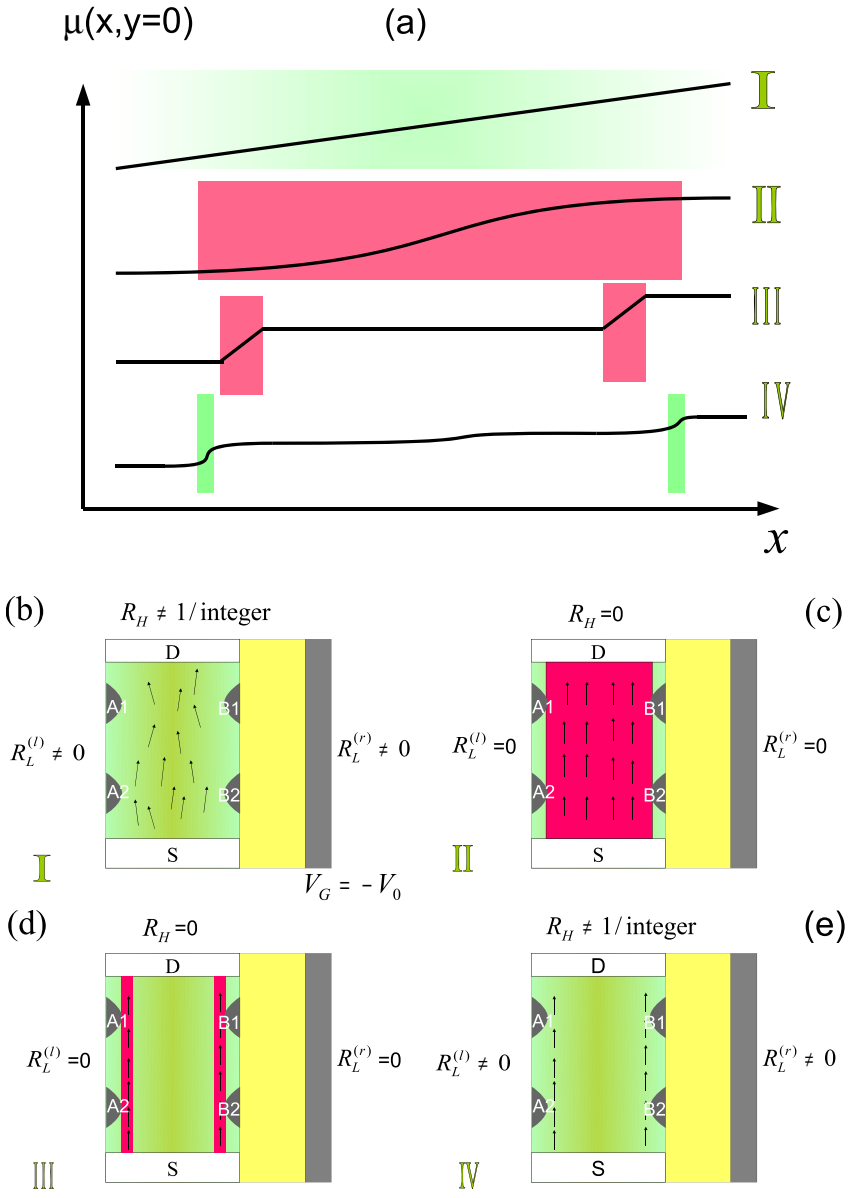

Figure 3. (a) The electrochemical potential distribution at a generic sample. The smooth potential is obtained by applying $-V_0$ to the side gate. The illustration resembles the experimental and theoretical calculations (see the related text). The Roman numerals depict four different cases: case I, the system is completely compressible; case II, the bulk is incompressible; case III, the incompressible strips reside at the edges; and case IV, the 'evanescent' incompressible strips reside at the edges. Shaded areas mark the current flowing regions (compressible (light-green) or incompressible (dark-pink)). The corresponding density distributions, reproduced from numerical calculations, while varying the B field from high to low are shown in (b–e). The color gradient codes the electron density variation at compressible regions, whereas highlighted (pink) regions are incompressible. Arrows indicate the direction of excess current density. Self-consistent calculations can be found in [26].

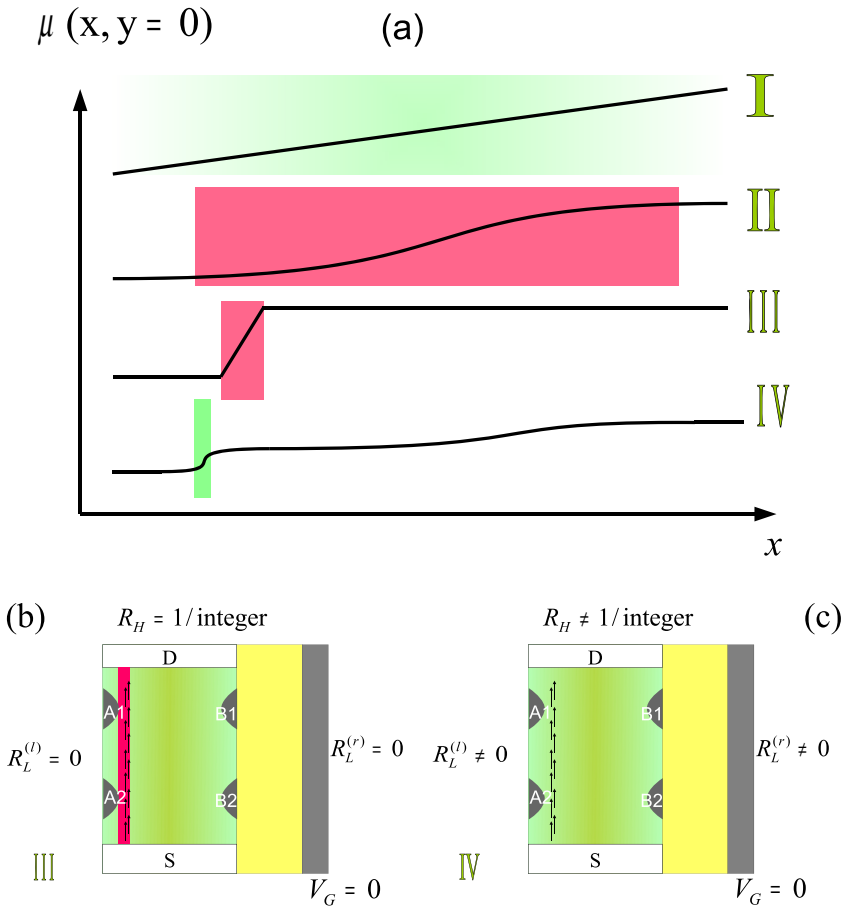

Figure 4. (a) The same as figure 3, but considering a CEO sample. The spatial distribution of incompressible strips and current density for cases III and IV.

The corresponding electrochemical potential distribution is shown in figure 4(a) where no incompressible strip resides at the CEO edge, together with the well-developed incompressible strip on the smooth edge (figure 4(b)) and the evanescent strip (figure 4(c)).

It is appropriate to summarize our discussion so far.

- Dipole strips emerge as a consequence of quantizing magnetic field and direct Coulomb interactions.
- Their widths and existences are determined by the electrostatic boundary conditions and DOS broadening.
- If these dipole strips become narrower than a few ℓ_B, they cease to be incompressible and charge can scatter across them in the presence of disorder. For relatively smooth confinements, the narrow width is due to local equilibrium fields. For sharp confinements (e.g. infinite wall at a boundary), the dipole strips are never incompressible at any field range.
- If an incompressible region resides at the bulk of the sample and its properties are solely determined by the disorder, this situation is called the bulk IQHE. The disorder is included to our calculations via DOS broadening.

- If the strip is at the edge and its properties are also affected by the boundary electrostatics, this situation is called the edge IQHE.

2.3. *Utilizing Ohm's law via local conductivities*

Next, we would like to highlight the essentials of the complementary transport calculations to elucidate IQHE within the screening theory. For further details see the comprehensive review by Gerhardts [50]. The self-consistent calculation of the electrostatic potential and the electron density distributions together with a local version of Ohm's law provides an explicit relation between the formation of the incompressible strips and the QHE [9]. The theory elucidates all the experimental findings reported at the local probe measurements. An important aspect of the screening theory is to prescribe an explicit calculation scheme to obtain the global resistances, starting from local conductivities. Here, we briefly mention the calculation scheme for obtaining local conductivities. The complementary transport calculations of screening theory assume Gaussian single-impurity potentials (i.e. disorder), as considered by Ando and co-workers within the self-consistent Born approximation (SCBA) [51–53]. Since the derivation of the DOS and conductivities has little relevance to our discussion and is a standard procedure, we provide only the results of local longitudinal and Hall conductivities,

$$\sigma_{\mathrm{H}}(x,y)=\frac{e^2}{h}\nu-2\frac{e^2}{h}\frac{\pi^2}{4}\sum_{n=0}^{\infty}\int \mathrm{d}E\left[-\frac{\partial f(E,V_{\mathrm{T}}(x,y))}{\partial E}\right]\frac{\Gamma_n^{yx}}{\hbar\omega_{\mathrm{c}}}[\Gamma_n^{yx}A_n(E)]^3 \tag{10}$$

and

$$\sigma_{\mathrm{L}}(x,y)=2\frac{e^2}{h}\frac{\pi}{2}\sum_{n=0}^{\infty}\int \mathrm{d}E\left[-\frac{\partial f(E,V_{\mathrm{T}}(x,y))}{\partial E}\right][\Gamma_n^{xx}A_n(E)]^2, \tag{11}$$

where the pre-factor 2 accounts for the spin degeneracy, n is the Landau index, $A_n(E)$ represents the spectral function and Γ_n^{xx}, Γ_n^{yx} are determined by the impurity parameters. The spectral function with a broadening Γ_n is given by

$$A_n(E)=\frac{2}{\pi\Gamma_n}\sqrt{1-\left(\frac{E-E_n}{\Gamma_n}\right)^2}, \tag{12}$$

which is centered around $\hbar\omega_{\mathrm{c}}(n+1/2)$ and assumes a semi-elliptic form. Note that each conductivity element has contributions from all levels below the Fermi energy. The above description of the conductivity tensor elements within the SCBA is guaranteed to preserve the Onsager relations [53].

To simplify our discussion, we assume the limit of short-range scatterers; then the coefficients assume the forms $(\Gamma_n/\Gamma)^2=1$, $(\Gamma_n^{xx}/\Gamma)^2=n+1/2$ and $(\Gamma_n^{yx}/\Gamma)^4=n+1/2$, where $\Gamma=4n_{\mathrm{I}}V_0^2/(2\pi\ell_B^2)$ is determined by the strength of the disorder via the impurity density n_{I} and the single-impurity potential amplitude V_0. By a straightforward substitution, the local conductivities can be prescribed in terms of the local filling factor, together with impurity parameters. Here, one can utilize the definition of the filling factor $\nu(x,y)=2\sum_{n=0}^{\infty}\int \mathrm{d}E\,A_n(E)\,f(E-\mu(x,y))$, where $\mu(x,y)$ is the position-dependent electrochemical potential. Note that the co-existence of the compressible and incompressible strips leads to a highly nonlinear system due to their different screening properties. To be explicit, if an external current is imposed a Hall potential will develop, and within the compressible strips it can be well screened, whereas in the incompressible strips it cannot be screened (see the discussion

in section 2.2). Therefore, within the (QH) regime there is no linear response, in the sense that the electrochemical potential, as observed in the scanning probe microscopy experiments [18, 19, 22], is position dependent considering the ballistic small-sample limit.

Recall that the screening theory provides local electrostatic potential and filling factors, self-consistently. Therefore, one can obtain the local conductivities within the SCBA for given system parameters. However, such a relation can also be obtained from different approaches [15, 54, 55]. We use the definition of the conductivity tensor given as

$$\hat{\sigma}(x, y) = \begin{pmatrix} \sigma_{\mathrm{L}}(x, y) & \sigma_{\mathrm{H}}(x, y) \\ -\sigma_{\mathrm{H}}(x, y) & \sigma_{\mathrm{L}}(x, y) \end{pmatrix}. \tag{13}$$

Since we are mainly interested in the transport properties of the incompressible strips, we confine our discussion to a situation where the Fermi energy (or the electrochemical potential at finite temperatures and in the presence of an external current) is in the single-particle gap. Then one can easily show that $\sigma_{\mathrm{L}}(\nu(x, y) = \text{integer}) = 0$ and $\sigma_{\mathrm{H}}(\nu(x, y) = \text{integer}) = \frac{e^2}{h}\nu(x, y)$. This behavior can be understood by the following line of argumentation: due to the absence of available states at the Fermi energy, there is no scattering within the incompressible regions; hence, the longitudinal conductivity vanishes. Meanwhile, the Hall conductivity is just proportional to the local electron density and quantum mechanical corrections vanish at integer filling factors (the second term in equation (10)); therefore it assumes a quantized value given by $\nu(x, y)$. At the compressible regions, the system behaves like a metal, i.e. σ_{L} is finite and σ_{H} varies approximately linearly with the applied B field. Note that the actual values of the conductivities at the compressible regions depend on the properties of the impurity and the approximation utilized. Based on the above brief discussion, we describe the local conductivities as

$$\sigma_{\mathrm{L}}(x, y) \begin{cases} = 0, & \nu(x, y) = \text{integer} \\ \neq 0, & \nu(x, y) = \text{non-integer} \end{cases}$$

and

$$\sigma_{\mathrm{H}}(x, y) = \frac{e^2}{h}\nu(x, y).$$

Before proceeding with the calculation of global quantities, we would like to clarify our above approach and discuss its validity regimes. First of all, replacing the local conductivities by the global ones (which are obtained for an unbounded system) is only valid if the length scale of the single-impurity potential is smaller than the density–density correlation length. In other words, the system should be ballistic, i.e. the sample length should be smaller than the mean free path. This condition also implies that utilizing the above-mentioned SCBA is only reasonable in the short-range impurity regime. As we consider. However, the analytical calculation schemes for obtaining local conductivities provided in the literature considering vortex states explicitly show that, as a first order approximation, replacing local conductivities by global ones is viable [56]. The second important issue is related to the SCBA itself; it is well known that this approximation is questionable to describe localization effects in the large-sample limit where the properties of the IQHE are determined by the bulk. In this work, we confine ourselves to a system where the samples are ballistic and are in the small-sample limit. This allows us to use the SCBA, keeping in mind that localization effects are not dominant. The above limitations and the details of local Ohm's law are discussed comprehensively in the original works of Gerhardts and co-workers [9, 15, 50].

Given the electron density, one can obtain the global resistances using the local Ohm's law, $\mathbf{j}(x, y) = \hat{\sigma}(x, y)\mathbf{E}(x, y)$, for an imposed external current I. It is also important to note that, throughout this work, we only deal with the excess current I injected from the contacts; however, the (chiral) equilibrium current I_{eq} is not considered. We assume that the injected current is much larger than the equilibrium current. The effect of I_{eq} will be discussed elsewhere. Since the longitudinal conductivity σ_{L} vanishes once the electronic system has a percolating incompressible strip *somewhere* in the sample, simultaneously the longitudinal resistivity and the electric field along the strip also vanish [15]. Therefore the excess current is confined to these incompressible regions if it exists.

In the following section, we discuss the influence of highly asymmetric lateral confinement on the current distribution. By highly asymmetric lateral confinement we mean that one side is CEO defined and the opposing edge is etch or gate defined. We also investigate the effects emanating from the injection contacts. We first assume that all the contacts are 'perfectly' ideal, i.e. the edge states are in equilibrium with the source and drain contacts. This picture changes if the contacts are non-ideal with finite reflection and transmission coefficients, and then one should reconsider the spatial distribution of the incompressible strips in front of the contacts [22, 26]. Therefore, one should include scattering events and/or the effect of the electric fields near the contacts and between the boundaries of compressible and incompressible regions.

3. Two edge regimes at four characteristic B fields, with ideal/non-ideal contacts

We begin by defining ideal and non-ideal contacts before proceeding with the discussion of their influence on the current distribution at CEO samples. An ideal contact fully equilibrates all incoming incompressible strip currents with the contact such that all outgoing incompressible strips have their outermost chemical potential set by the contact chemical potential. A non-ideal contact partially reflects some of the incoming chemical potential from one or more incompressible strips to the outgoing incompressible strips. In the language of the Landauer–Búttiker formalism [6], the incompressible strips are referred to as 'edge states', and the contacts are assigned reflection and transmission coefficients for each incompressible strip. These contacts thus become the defining components of the single-particle non-local conductance, where dissipation takes place due to equilibration. The next definition is that of a good ohmic contact whose resistance is much smaller than the other measured resistances in the problem. Explicitly, a non-ideal contact can still be ohmic if the contact resistance remains below other resistance scales. Once the contact resistance becomes dominant, it is called a bad or non-ohmic contact. A detailed discussion of ideal/non-ideal and ohmic/non-ohmic contacts can be found in [22].

Early scanning probe experiments [19] and very recent comprehensive investigations [22, 57] using various experimental methods show that there is a depleted electron density just in front of the metallic contacts. This density gradient induces finite scattering between the current channel(s) and the contacts, yielding a non-ideal contact. Despite the low electron density region, it is shown that state of the art contacts are perfectly ohmic [22]. It is only recently that the self-consistent calculations by Eksi *et al* [26] could provide a quantitative description of the electron-poor region in front of the contacts. This calculation scheme also presents the formation of compressible/incompressible strips in front of the contact. These non-ideal contact ideas are further supported by other recent theoretical investigations considering contacts [58, 59].

Here we phenomenologically investigate the edge-to-bulk transition of the IQHE considering a sample defined on a CEO crystal, considering both ideal and non-ideal ohmic contacts. Following the discussion in section 2.2, we repeat the simplified definition: if the properties of the incompressible strips are defined by the edge profile, this situation is called the edge IQHE or small-sample limit, whereas if the incompressible strip or region resides at the bulk with conductance properties solely described by disorder, we call this situation the bulk IQHE or large-sample limit. For convenience we neglect the spin degree of freedom, since the effects we describe are universal, i.e. independent of whether Landau or Zeeman energies create the single-particle gap and the subsequent incompressible strip. Therefore, we only deal with even-integer filling factors, i.e. $\nu = 2k$ $(k = 1, 2, 3, \ldots)$.

3.1. Ideal contacts

Once the sample geometry is given, conductance properties will be determined by the electron distribution within the sample and near the contacts. In the case of ideal contacts, it is assumed that there is no density gradient in the close vicinity of the contacts. Therefore the incompressible strips are formed only due to the lateral confinement and are equilibrated with the contacts, without reflections. Hence, scattering between the current contacts (S, D) and the incompressible strips is completely suppressed. As a first step we consider such ideal contacts at the ends of our sample. We depict the positions and the existence of incompressible strips considering four characteristic B fields in descending order in figures 3(b)–(d). Here we consider a generic sample, i.e. both edges are relatively smooth. At sufficiently high magnetic fields and neglecting correlation effects, the lowest Landau level is partially occupied (figure 3(b)). Hence, the electronic system is completely compressible (shown by color graded regions). Consequently, the global resistances R_{L}, R_{H} are both finite, and excess current is distributed all over the sample, case I. The conductivities can be described by the Drude model [60]. The small deviations of the arrow directions from the electric field direction are to demonstrate the scattering processes. Once the field is lowered (figure 3(c), case II), a large bulk incompressible region is formed and the excess current is confined to this region, where no (back)scattering is present. Hence, all arrows are directed along the applied current direction. The longitudinal resistances measured on both edges vanish and the Hall resistance is quantized. Lowering the B field results in the formation of two edge incompressible strips (case III) and once more the imposed current is confined to these strips (figure 3(d)). At the lowest B field considered here, the current is essentially confined to the *evanescent* of the incompressible strips, as depicted in figure 3(e). However, some of the current is also distributed to the bulk of the sample. The ratio of current flowing from the evanescent incompressible strips and bulk decreases while lowering the B field and case I is recovered before the next filling factor plateau sets in.

Next, we consider the current distribution at a CEO sample considering the sharp edge on the right-hand side in figures 4(b) and (c). Cases I and II remain unaffected by the sharp edge and are therefore not shown. In contrast to the smooth edge, the current distribution is strongly altered once the edge IQHE regime sets in, cases III and IV. The excess current is essentially confined to the left edge. Direct measurement of such a distinction between CEO and generic samples is possible via the scanning probe experiments. Unfortunately, an experimental investigation of the electrochemical potential distribution at CEO samples is not available in the literature. Despite this fact, one can trace the signature of such an asymmetry at the potential

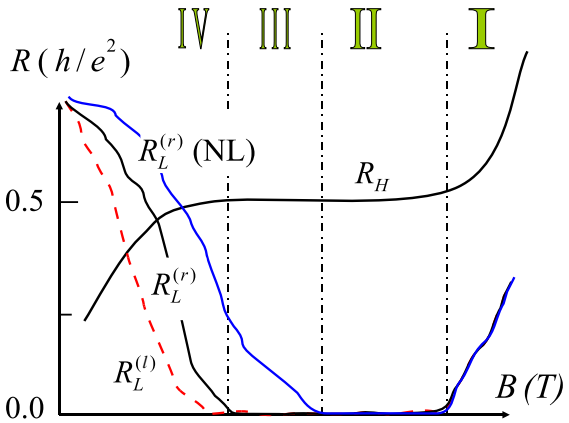

Figure 5. The predicted global resistances as a function of magnetic field when the measurements are carried out at sufficiently low temperatures. The longitudinal resistances predicted at the smooth edge $R_{\mathrm{L}}^{(l)}$ (broken line), at the sharp edge in the linear transport regime $R_{\mathrm{L}}^{(r)}$ (black solid) and at the nonlinear regime $R_{\mathrm{L}}^{(r)}(NL)$ (blue solid line). In order to suppress the effect of long-range potential fluctuations high-mobility wafers should be considered. Similar results obtained by self-consistent calculations at asymmetric gate-defined samples can be found in [16].

distributions, where one edge is etched and the opposing edge is gate defined [19, 61]. One can see that the potential distribution is symmetric if both the edges are etched, whereas if a contact resides on one edge, the potential distribution is smoother on this side. Although there is evidence that the boundary conditions influence the electrochemical potential distribution, performing local probe experiments at CEO samples would clarify our discussion. This is our first experimental proposal.

Alternatively, one can also measure the global resistances at the CEO sample, and indirectly measure the differences between the generic sample and the CEO sample. We expect (almost) no differences between the global resistances when comparing the generic and the CEO sample at the highest B fields, cases I and II. For case I, the system is in a complete compressible state; hence, the external potential is almost perfectly screened and transport is determined by the metallic bulk. As a result, there is no apparent difference between the CEO and generic samples when measuring the resistances. A similar argumentation also holds for case II; in contrast to the previous case, in this situation the transport properties are imposed by the bulk incompressible region, which is not affected by the boundary conditions, i.e. the longitudinal resistance vanishes for both systems $R_{\mathrm{L}}^{(g)} = R_{\mathrm{L}}^{(\mathrm{CEO})} = 0$. The above arguments only hold for very-high-mobility samples, where no long-range potential fluctuations exist due to disorder. The situation remains unchanged for case III, since the incompressible strip on the left side of the CEO sample still decouples opposing (probe) contacts. Consider case IV, where the edge incompressible strips at both samples become evanescent. In this case, the current distributions are affected by the edge profile. Therefore the measured resistances differ at the lower edges of the plateau. This distinction is obliterated once case I is recovered, i.e. when the evanescent incompressible strips completely vanish. Figure 5 shows the expected R_{H} (thick solid line), $R_{\mathrm{L}}^{(r)}$ (thin broken line) and $R_{\mathrm{L}}^{(l)}$ (thin solid line) for the CEO sample. Note that $R_{\mathrm{L}}^{(l)}$ corresponds to the longitudinal resistance of a generic sample; meanwhile, $R_{\mathrm{L}}^{(r)}$ measures the transport at the

CEO edge. This is an indirect way to measure the effect of different boundary conditions on transport. Again, unfortunately, it is very difficult to deposit working contacts exactly on the top of the CEO edge, experimentally. Therefore, observing such a difference due to boundary conditions is obscured. As we will show below, the solution to this difficulty is hidden in the symmetry of the IQHE.

We will now discuss dc current polarity effects for distinguishing the CEO edge from the generic case. Let us first consider a generic sample, and impose a positive dc current such that the electrochemical potential looks as it is shown in figure 3(a). That is, the right side has a higher potential energy. Once the current amplitude is increased, the left incompressible strip becomes narrower, due to the fact that there are more electrons on the left-hand side to screen the external potential compared to equilibrium. Another way to see this effect is to consider the electric field within the strip; on the left side the total potential variation is $|eV_{\rm SD}/2+\hbar\omega_{\rm c}|$ and on the opposing side the variation is $|eV_{\rm SD}/2-\hbar\omega_{\rm c}|$, where we assumed that the current is shared among the two incompressible strips equally. Here, $\hbar\omega_{\rm c}$ emanates from the equilibrium current. One can see from equation (9) that, at higher electric fields, the single-particle gap becomes effectively smaller; hence, the gapped region is reduced. The transport consequence is that the incompressible strip width shrinks. On the opposing edge, the incompressible strip is enlarged to maintain electrostatic stability. Once the current amplitude is sufficiently large the left incompressible strip collapses. A detailed calculation can be found in [31]. The effect described is a natural result of self-consistency and is predicted by numerical calculations [15]. If we alter the current direction, the potential distribution will look the same; however, the opposing edges will be swapped, i.e. the left side will be elevated. Thus, there is no measurable dc polarity dependence on the global resistance in generic samples.[6]

Nonetheless, dc polarity has an important influence on asymmetric samples such as the CEO samples. The explicit self-consistent calculations considering an asymmetric sample predict that the width of the magnetic field intervals in which IQHE is observed can be tuned by changing the current direction [16]. This prediction is tested successfully at gated samples; however, tuning the visibility of the IQHE is limited to the nonlinear transport regime [25]. Since it is not possible to manipulate the edge steepness arbitrarily via gates. In contrast to gate-defined Hall bars, at CEO samples one side serves as an infinite wall; hence, one can tune the visibility of the IQHE in a wider experimental parameter window and more strikingly even at the linear transport regime. From the experimental point of view, it is clear that performing such experiments is highly challenging and requires expertise regarding the CEO samples. At the moment, the experimental difficulty is surpassed and preliminary results agree well with the theoretical predictions [62].

To sum up: in the case of ideal contacts we have seen that the bulk-to-edge transition can be measured with local probe experiments investigating the electrochemical potential profiles. However, one cannot resolve the difference between the edge (case III) and bulk (case II) regimes of the QHE simply by measuring the global resistances. We expect to observe a difference only at the lower edge of the plateau regime. In addition, we proposed measurements of the global resistances at the CEO samples, imposing a dc current with opposite polarities to observe the influence of the boundary conditions on transport. To observe the different regimes of the QHE, one can also consider non-ideal contacts and carry out standard QHE measurements. We discuss this case in the following subsection.

[6] In fact, this effect is known to the experimentalists and named the hot-edge effect.

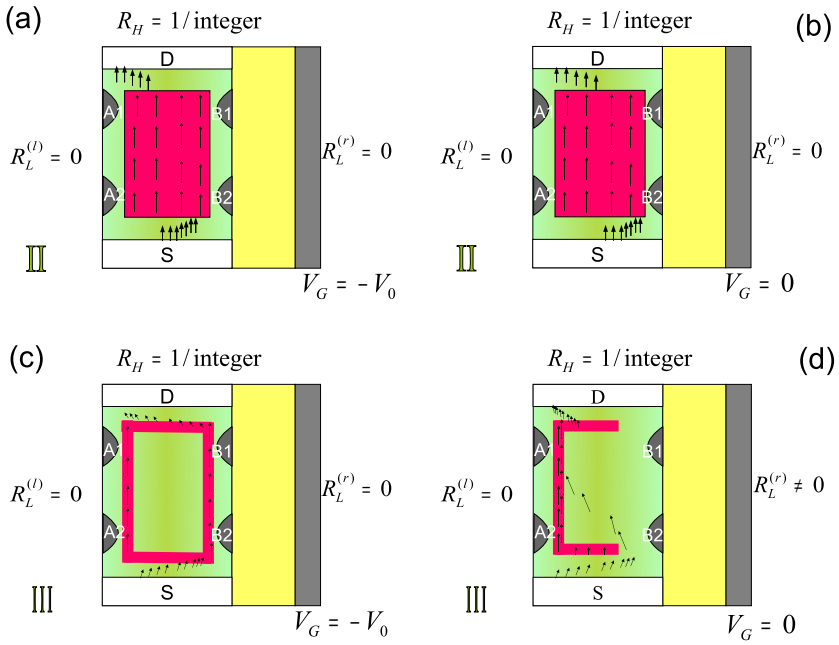

Figure 6. Schematic drawing of incompressible strips and current densities considering a generic sample (left panel) and a CEO sample, while contacts are non-ideal. The location of the hot-spots depend on the field direction (see related text). The scattered arrows shown in (d) indicate the bulk current, which diminishes the visibility of the QH resistance.

3.2. Non-ideal contacts

The essential difference between an ideal and a non-ideal contact is the electron-poor region in the close proximity of the contacts. As mentioned before, recent experimental findings show that one cannot model a contact simply by placing a metallic gate representing an equipotential on the surface. It was found that the contacts behave like fingers inserted into the 2DEG, where fingers are metallic and the space between them is insulator-like [22, 57]. As a consequence, the 2DEG is partially depleted from the contacts and a density gradient is formed in front of them. Such a density gradient leads to decoupling of the incompressible strips from the contacts. We compare the spatial distribution of the incompressible strips and current distribution for cases II and III in figure 6, also taking into account the density gradient near the contacts. The left panel depicts a generic sample, whereas the right panel shows a CEO sample. Different from the ideal contact situation, now the incompressible region (case II) or strip (case III) can only come near the contact, whereas the region between the contact and incompressible region is compressible. This implies that scattering is finite and the transmission probability from a contact to the incompressible strip is no longer unity. Remarkably, for the non-ideal contact at the CEO sample, some of the current can also be scattered to the bulk of the sample in case III. The amount of bulk current is directly proportional to the quality of the contact. This scattered bulk current is re-collected by the incompressible strip at the left side, once the electrochemical equilibrium is restored. The longitudinal resistance at the left side is always zero due to the well-developed incompressible strip. In contrast, one can still measure a finite R_L on the right side. Interestingly, the Hall resistance will deviate from its quantized value due to the small

amount of bulk current, if measured between contacts A2 and B2, whereas if R_H is measured between A1 and B1 it is quantized, since at this location all the current is now confined to the edge incompressible strip. Such a behavior is not observed at a generic sample due to lateral symmetry. In addition, if the bulk is completely incompressible (case II), then the current is directly collected by the bulk region, for both samples. This difference between case II and case III manifests the distinction between the bulk IQHE and the edge IQHE. The former is only determined by the bulk properties of the conductivity model, namely by disorder, and the latter is determined by boundary conditions. If both edges of our sample are defined by CEO, then one can only observe the bulk IQHE. By depositing metallic gates on both sides and varying the steepness of the edge, one should be able to tune the width of the IQHE plateaux by softening the sharp edges with negative gate biases. This is our third experimental proposal.

4. Other symmetries of the system

In this section, we consider only the non-ideal contact configuration, which is relevant for real experimental systems, and assume a clean sample without any long-range potential fluctuations in the small-sample limit. Recall that the effect of disorder is included in our model via the conductivity model we employ. The equilibration processes are investigated based on the formation of incompressible strips. Our arguments are supported by some experiments that investigated the effects of incompressible strips on the equilibration and decoupling of the system [63, 64]. The term 'decoupling' is used to express electrochemical and thermodynamical non-equilibrium; that is, the electrons cannot be redistributed easily due to the strip and have different electrochemical potentials on opposing edges.

Here, we mention two different ways of breaking the symmetry of the system, as set by the external B field. This is different from the symmetry breaking effects due to current (electric field), discussed before. First, we investigate the hysteresis effects that can arise. We compare the decoupling properties of the edge incompressible strip with those of the bulk incompressible strip, hence the bulk-to-edge IQHE transition. Next, using the findings of experimental and theoretical investigations considering hot-spots, we alter the direction of the external magnetic field and search for observable differences at transport.

4.1. Sweep direction-induced hysteresis

Let us conceive an experiment for the generic sample, in which one starts from low fields and ends the measurement on an upsweep at a field such that the lowest Landau level is partially occupied. In such a measurement the case sequence is IV–III–II–I. First the current is flowing from both sides along the evanescent incompressible strips and the system is compressible. At a higher field (case III) the system will develop edge incompressible strips, which decouple the bulk from the edges. In this case, the bulk electrons have a different electrochemical potential compared to edges. Bulk is not accessible for the edge electrons and edge is not accessible for the bulk electrons. When increasing the B field, edge incompressible strips become wider to keep the electrostatic stability, until the bulk becomes completely incompressible (case II). Here, the edges are decoupled by the bulk incompressible region. Further increase of the field strength results in the disappearance of the bulk incompressible region, hence case I. If one now sweeps the field down, the opposite behavior will be observed. The change in the sweep direction obviously has no influence on resistance measurements for the generic samples. Instead, one

can measure the equilibration process at generic samples by means of a single-electron transistor (SET) residing at the top surface [63]. It is shown that thermodynamic equilibration is hindered by the incompressible regions and the magnetic field sweep direction induces a strong hysteresis on the local electrochemical potential distribution. At temperatures below 0.1 K, the relaxation time is reported to be as long as hours. Similar observations of a strong hysteresis at the resistances of the passive layer are reported for the bilayer systems [40, 64] and is elucidated by self-consistent screening calculations [41].

Now let us consider the CEO sample, where only one incompressible strip resides at the left edge. The compressible bulk is accessible for electrons to restore equilibrium, due to the absence of right strip. Therefore, while sweeping up, equilibrium can be achieved easily; however, while sweeping down, the bulk incompressible region hinders equilibration. To be explicit, during down-sweep the bulk incompressible region freezes the potential landscape and equilibration is suppressed. Turned around, once the bulk incompressible region is formed it stays for large B intervals. At the opposite sweep direction one starts with a narrow incompressible strip at the left edge, which cannot effectively decouple bulk; therefore the potential landscape is not frozen for large B intervals. It is apparent that sweep direction has an influence on the equilibration process. Consequently, down-sweep presents a larger IQHE (i.e. bulk and edge together), whereas up-sweep only shows the edge IQHE. This induces different paths for the longitudinal resistance when sweeping up or down, namely a hysteresis. In addition, the visibility of this hysteresis strongly depends on the potential profile at the bulk; hence the role of long-range fluctuations has to be taken into account. Such a potential freezing model is applied to the bilayer system and the observed hysteresis is elucidated [40, 41]. There the effect of long-range fluctuations is also examined in detail, showing that the visibility of hysteresis is enhanced if the system has sufficiently strong long-range potential fluctuations. It is also discussed that if the sample is large the edge effects are suppressed completely. As a simple test, one can erase the memory of the system by warming up the sample during down-sweep, at the hysteresis interval. The warming process will melt the bulk incompressible region and therefore the system comes to the equilibrium state. Afterwards, one can measure the R_L and check if it is still in the IQHE regime. Such a test is done at the bilayer systems and it is observed that the hysteresis vanishes, similarly to what we would expect for the CEO samples.

Note that for an ideal contact, one incompressible strip is sufficient to decouple opposing edges, and sweep direction is not important. However, we propose that the visibility of the hysteresis should also depend on the quality of the non-ideal contact. To be explicit, if the contact approximates to an ideal contact the hysteresis should disappear.

4.2. The orientation of the B field

The other interesting symmetry breaking is due to the formation of *hot-spots*, known for a while experimentally [18, 22, 65] and also calculated recently [26, 59]. The hot-spot is on either the left or right bottom near the injection contact, depending on the field direction. At the drain contact, it is located at the diagonal corner[7]. It is apparent that the formation of hot-spots has no influence on the resistances measured far from the contacts at a generic sample. Remarkably, at a CEO sample the location of hot-spots alters the equilibration process of the excess current. Consider figure 6(d); if the B field is directed along the positive z-axis, the hot-spot is at the right bottom corner of the sample. Hence, some of the excess current can be scattered to the

[7] Cf figures 6 and 2(b) of [26] for actual calculations.

bulk compressible region, resulting in deviations from the QH resistance, if it is measured using contacts A2–B2. Correlatively, the R_L is finite on the right side. This situation has already been discussed in the previous section. Next we alter the B field orientation to the negative z-direction; then the hot-spot will form on the left bottom corner of the sample. Consequently, the excess current is directly confined to the left incompressible strip. Hence, R_H^{A2-B2} is quantized and R_L^{B1-B2} vanishes. This behavior has implications on the hysteresis discussed above, since the equilibration process is also affected. Our model predicts that if a hysteresis is observed at the CEO sample, the different paths should alternate depending on the field direction, since the location of the hot-spots will also be altered and current injection process will be strongly affected.

5. Conclusion

In this work, we have investigated the effects of a sharp boundary on the transport properties and the electrochemical potential distribution of a cleaved edge overgrown sample. First, we reintroduced the calculation scheme for obtaining electron and potential distributions, starting from analytical electrostatic formulation, and extended our discussion to the self-consistent calculation scheme. The effects of boundaries, together with interactions, on the formation of incompressible strips were discussed based on the literature and supported by self-consistent calculations. We showed that the incompressible strip does not exist at the sharp edge, agreeing with previous calculations and experiments. In the next step, we summarized the essential findings of two sets of experiments relevant to our discussions on the electrochemical potential distribution at narrow samples and regarding the cleaved edge overgrown samples. The basis of the complementary transport calculations of the screening theory was briefly reintroduced in section 2.3. Equipped with the theoretical and experimental findings, we investigated the current distribution, comparing generic and cleaved edge overgrown samples. We considered ideal and non-ideal contacts, together with the influence of current direction on the global resistances. In section 4, the effects of sweep direction and B-field orientation were discussed. Several experimental predictions emanated from our discussions due to the sharp edge; these can be summarized as follows.

- At local probe experiments, one cannot observe an electrochemical potential drop at the sharp edge.
- The visibility of the IQHE should be tuned by imposing dc currents in different directions, under the same experimental conditions.
- If both sides of the Hall bar are defined by sharp edges, only the bulk IQHE can be observed. In addition, we predict that by making the edge smoother plateaux should be extended.
- We predict that, at the edge IQHE regime, equilibration processes are promoted due to the absence of the incompressible strip at the sharp edge and are suppressed at the bulk IQHE regime by virtue of the large incompressible region at the bulk. Hence, sweeping the magnetic field direction should induce a hysteresis on global resistances, which is strongly affected by the long-range fluctuations and contact quality.
- Altering the orientation of the B field also alters the spatial locations of the hot-spots; thus, altering the field orientation should strongly affect the hysteresis.

Once the sharp edge behaves like a hard-wall potential, the 1D edge channels proposed by Halperin [5] and Búttiker [6] should form and the edge profile should not be important. This seems to be the case for equilibrium, namely when there is no external current. However, the screening theory states that if the width of the incompressible edge strip becomes narrower than a few magnetic lengths, scattering is promoted. In the case of an external current the incompressible strip collapses if one analytically calculates the effect of local electric fields on the local DOS. If the incompressible strip vanishes, then the longitudinal resistance becomes finite. Hence, the IQHE disappears.

As a final remark, similar asymmetries of the QH and the longitudinal resistances were recently reported both experimentally [25, 44, 48, 62] and theoretically [16, 66], all attributed to the direct Coulomb interaction. In [16], it is predicted that due to the nonlinear effects induced by the imposed large current, the widths of the incompressible strips are enhanced (or reduced), which, we believe, can be exploited in magnifying the asymmetrical behaviors we have discussed.

Acknowledgments

We thank Húseyin Kaya for his support in organizing the first 'Akyaka Nano-electronics Symposium' and the Feza–Gúrsey Institute for the fourth, where this work was partially conducted. The I.T.A.P.-Marmaris is also acknowledged for organizing the winter school where the discussions on utilizing the CEO crystals were initiated. This work was partially supported by Túbitak (109T083) and the Istanbul University projects department (BAP-6970).

References

[1] Klitzing K V, Dorda G and Pepper M 1980 New method for high-accuracy determination of the fine-structure constant based on quantized Hall resistance *Phys. Rev. Lett.* **45** 494
[2] Halperin B I, Stern A, Neder I and Rosenow B 2011 Theory of the Fabry–Perot quantum Hall interferometer *Phys. Rev.* B **83** 155440
[3] Laughlin R B 1981 Gauge gedanken experiment iqhe *Phys. Rev.* B **23** 5632
[4] Kramer B, Kettemann S and Ohtsuki T 2003 Localization in the quantum Hall regime *Physica* E **20** 172
[5] Halperin B I 1982 Self-consistent local-equilibrium model for density profile and distribution of dissipative currents in a Hall bar under strong magnetic fields *Phys. Rev.* B **25** 2185
[6] Búttiker M 1986 Four-terminal phase-coherent conductance *Phys. Rev. Lett.* **57** 1761
[7] Chklovskii D B, Shklovskii B I and Glazman L I 1992 Electrostatics of edge states *Phys. Rev.* B **46** 4026
[8] Chang A M 1990 A unified transport theory for the integral and fractional quantum hall effects: phase boundaries, edge currents and transmission/reflection probabilities *Solid State Commun.* **74** 871
[9] Siddiki A and Gerhardts R R 2004 Incompressible strips in dissipative Hall bars as origin of quantized Hall plateaus *Phys. Rev.* B **70** 195335
[10] Gelfand B Y and Halperin B I 1994 Edge electrostatics of a mesa-etched sample and edge-state-to-bulk scattering rate in the fractional quantum Hall regime *Phys. Rev.* B **49** 1862–6
[11] Oh J H and Gerhardts R R 1997 Self-consistent Thomas–Fermi calculation of potential and current distributions in a two-dimensional Hall bar geometry *Phys. Rev.* B **56** 13519
[12] Arslan S, Cicek E, Eksi D, Aktas S, Weichselbaum A and Siddiki A 2008 Modeling of quantum point contacts in high magnetic fields and with current bias outside the linear response regime *Phys. Rev.* B **78** 125423
[13] Lier K and Gerhardts R R 1994 Self-consistent calculation of edge channels in laterally confined two-dimensional electron systems *Phys. Rev.* B **50** 7757

[14] Kanamaru S, Suzuuara H and Akera H 2006 Spatial distributions of electron temperature in quantum Hall systems with compressible and incompressible strips *J. Phys. Soc. Japan* **75** 064701–10
[15] Gúven K and Gerhardts R R 2003 Self-consistent local-equilibrium model for density profile and distribution of dissipative currents in a Hall bar under strong magnetic fields *Phys. Rev.* B **67** 115327
[16] Siddiki A 2009 Current-direction-induced rectification effect on (integer) quantized Hall plateaus *Euro. Phys. Lett.* **87** 17008–14
[17] Wei Y Y, Weis J, Klitzing K V and Eberl K 1998 Edge strips in the quantum Hall regime imaged by a single-electron transistor *Phys. Rev. Lett.* **81** 1674
[18] Ahlswede E, Weitz P, Weis J, von Klitzing K and Eberl K 2001 Hall potential profiles in the quantum Hall regime measured by a scanning force microscope *Physica* B **298** 562
[19] Ahlswede E, Weis J, von Klitzing K and Eberl K 2002 Hall potential distribution in the quantum Hall regime in the vicinity of a potential probe contact *Physica* E **12** 165
[20] Huber M, Grayson M, Rother M, Biberacher W, Wegscheider W and Abstreiter G 2005 Structure of a single sharp quantum Hall edge probed by momemtum-resolved tunneling *Phys. Rev. Lett.* **94** 016805
[21] Huber M, Grayson M, Rother M, Deutschmann R A, Biberacher W, Wegscheider W, Bichler M and Abstreiter G 2002 Tunneling in the quantum Hall regime between orthogonal quantum wells *Phys. E Low-Dimens. Syst. Nanostruct.* **12** 125–8
[22] Dahlem F, Ahlswede E, Weis J and Klitzing K V 2010 Cryogenic scanning force microscopy of quantum Hall samples: adiabatic transport originating in anisotropic depletion at contact interfaces *Phys. Rev.* B **82** 121305
[23] Deviatov E V, Lorke A, Biasiol G, Sorba L and Wegscheider W 2010 Local investigation of the energy gap within the incompressible strip in the quantum Hall regime *Sov. J. Exp. Theor. Phys. Lett.* **92** 67–70
[24] Sailer J, Wild A, Lang V, Siddiki A and Bougeard D 2010 Quantum Hall resistance overshoot in two-dimensional (2D) electron gases: theory and experiment *New J. Phys.* **12** 113033
[25] Siddiki A, Horas J, Kupidura D, Wegscheider W and Ludwig S 2010 Asymmetric nonlinear response of the IQHE *New J. Phys.* **12** 113011
[26] Eksi D, Kilicoglu O, Góktas O and Siddiki A 2010 Screening model of metallic nonideal contacts in the integer quantized Hall regime *Phys. Rev.* B **82** 165308
[27] Pfeiffer L, West K W, Stormer H L, Eisenstein J P, Baldwin K W, Gershoni D and Spector J 1990 Formation of a high quality two-dimensional electron gas on cleaved GaAs *Appl. Phys. Lett.* **56** 1697–9
[28] Siddiki A and Gerhardts R R 2003 Thomas–Fermi–Poisson theory of screening for laterally confined and unconfined two-dimensional electron systems in strong magnetic fields *Phys. Rev.* B **68** 125315
[29] Morse P M and Feshbach H 1953 *Methods of Theoretical Physics* vol II (New York: McGraw-Hill) p 1240
[30] Suzuki T and Ando T 1993 Transport properties between quantum Hall plateaus *J. Phys. Soc. Japan* **62** 2986
[31] Gulebaglan S E, Sokmen I, Siddiki A and Gerhardts R R 2011 Local density of states of two-dimensional electron systems under strong in-plane electric and perpendicular magnetic fields arXiv:1105.2026
[32] Avishai Y and Montambaux G 2008 Semiclassical analysis of edge state energies in the integer quantum Hall effect *Eur. Phys. J.* B **66** 41–9
[33] Montambaux G 2011 Semiclassical quantization of skipping orbits *Eur. Phys. J.* B **79** 215–24
[34] Wulf U, Gudmundsson V and Gerhardts R R 1988 Screening properties of the two-dimensional electron gas in the quantum Hall regime *Phys. Rev.* B **38** 4218
[35] Dempsey J, Gelfand B Y and Halperin B I 1993 Electron–electron interactions and spontaneous spin polarization in quantum Hall edge states *Phys. Rev. Lett.* **70** 3639–42
[36] Ihnatsenka S and Zozoulenko I V 2006 Magnetosubband and edge state structure in cleaved-edge overgrown quantum wires in the integer quantum Hall regime *Phys. Rev.* B **74** 075320
[37] Weichselbaum A and Ulloa S E 2003 Potential landscapes and induced charges near metallic islands in three dimensions *Phys. Rev.* E **68** 056707
[38] Eksi D, Cicek E, Mese A I, Aktas S, Siddiki A and Hakioglu T 2007 Theoretical investigation of the effect of sample properties on the electron velocity in quantum Hall bars *Phys. Rev.* B **76** 075334

[39] Siddiki A 2009 Current-direction-induced rectification effect on (integer) quantized Hall plateaus *Europhys. Lett.* **87** 17008
[40] Siddiki A, Kraus S and Gerhardts R R 2006 Screening model of magnetotransport hysteresis observed in bilayer quantum Hall systems *Physica* E **34** 136
[41] Siddiki A 2007 Self-consistent coulomb picture of an electron–electron bilayer system *Phys. Rev.* B **75** 155311
[42] Gúven K, Siddiki A, Krishna P M and Hakioğlu T 2008 A self-consistent microscopic model of Coulomb interaction in a bilayer system as an origin of drag effect phenomenon *Phys. E Low-Dimens. Syst. Nanostruct.* **40** 1169–71
[43] Siddiki A and Marquardt F 2007 Self-consistent calculation of the electron distribution near a quantum-point contact in the integer quantum Hall effect *Phys. Rev.* B **75** 045325
[44] Siddiki A, Horas J, Moser J, Wegscheider W and Ludwig S 2009 Interaction-mediated asymmetries of the quantized Hall effect *Europhys. Lett.* **88** 17007
[45] Mares J J, Siddiki A, Kindl D, Hubik P and Kristofik J 2009 Electrostatic screening and experimental evidence of a topological phase transition in a bulk quantum Hall liquid *New J. Phys.* **11** 083028
[46] Friedland K-J, Siddiki A, Hey R, Kostial H, Riedel A and Maude D K 2009 Quantum Hall effect in a high-mobility two-dimensional electron gas on the surface of a cylinder *Phys. Rev.* B **79** 125320
[47] Siddiki A, Horas J, Kupidura D, Wegscheider W and Ludwig S 2010 Asymmetric nonlinear response of the quantized Hall effect *New J. Phys.* **12** 113011
[48] Horas J, Siddiki A, Moser J, Wegscheider W and Ludwig S 2008 Investigations on unconventional aspects in the quantum Hall regime of narrow gate defined channels *Phys. E Low-Dimen. Syst. Nanostruct.* **40** 1130–2
[49] Siddiki A and Gerhardts R R 2004 The interrelation between incompressible strips and quantized Hall plateaus *Int. J. Mod. Phys.* B **18** 3541
[50] Gerhartds R R 2008 Edge electrostatics of a mesa-etched sample and edge-state-to-bulk scattering rate in the fractional quantum Hall regime *Phys. Status Solidi b* **245** 378
[51] Ando T, Matsumoto Y and Uemura Y 1975 *J. Phys. Soc. Japan* **39** 279
[52] Ando T and Uemura Y 1974 *J. Phys. Soc. Japan* **36** 959
[53] Ando T, Fowler A B and Stern F 1982 Electronic properties of two-dimensional systems *Rev. Mod. Phys.* **54** 437
[54] Gerhardts R R 1975 Path-integral approach to the two-dimensional magneto-conductivity problem. II Application . . . *Z. Phys.* B **21** 285
[55] Aidala K E, Parrott R E, Kramer T, Heller E J, Westervelt R M, Hanson M P and Gossard A C 2007 Imaging magnetic focusing of coherent electronwaves *Nat. Phys.* **3** 464
[56] Champel T, Florens S and Canet L 2008 Microscopics of disordered two-dimensional electron gases under high magnetic fields: equilibrium properties and dissipation in the hydrodynamic regime *Phys. Rev.* B **78** 125302
[57] Goektas O 2009 Small alloyed ohmic contacts to 2DES and submicron scale Corbino devices in strong magnetic fields: observation of a zero bias anomaly and single-electron charging *PhD Thesis* Stuttgart University
[58] Uiberacker C, Stecher C and Oswald J 2009 Systematic study of nonideal contacts in integer quantum Hall systems *Phys. Rev.* B **80** 235331
[59] Kramer T, Krueckl V, Heller E J and Parrott R E 2009 On the self-consistent calculation of electric potentials in Hall devices arXiv:0911.4886
[60] Ashcroft N W and David Mermin N 1976 *Solid State Physics* (London: Brooks Cole)
[61] Ahlswede E 2002 Potential- und stromverteilung beim Quanten-Hall-Effekt bestimmt mittels Rasterkraft-mikroskopie *PhD Thesis* Universität Stuttgart
[62] Zhou C, Grayson M, Steinke L, Uccelli E, Koblmueller G, Bichler M, Abstreiter G, Schmult S and Dietsche W 2010 Quantum Hall effect at a tunably sharp cleaved-edge potential *APS Meeting Abstracts* p 25014

[63] Huels J, Weis J, Smet J, Klitzing K V and Wasilewski Z R 2004 Long time relaxation phenomena of a two-dimensional electron system within integer quantum Hall plateau regimes after magnetic field sweeps *Phys. Rev.* B **69** 085319

[64] Pan W, Reno J L and Simmons J A 2004 Hysteresis in the quantum Hall regimes in electron double-quantum structures *Int. J. Mod. Phys.* B **18** 3671–6

[65] Dietsche W, von Klitzing K and Ploog K 1996 Potential drops across quantum hall effect samples—in the bulk or near the edges? *Surf. Sci.* **361/362** 289

[66] Eksi D, Kilicoglu O, Aktas S and Siddiki A 2010 The current polarization rectification of the integer quantized Hall effect *Phys. E Low-Dimens. Syst. Nanostruct.* **42** 1066–8